

Narrow Line Seyfert 1 galaxies at hard X-rays^{*}

F. Panessa^{1†}, A. De Rosa¹, L. Bassani², A. Bazzano¹, A. Bird³, R. Landi²,
A. Malizia², G. Miniutti⁴, M. Molina⁵, P. Ubertini¹

¹*Istituto di Astrofisica Spaziale e Fisica Cosmica (IASF-INAF), via del Fosso del Cavaliere 100, 00133 Roma, Italy*

²*Istituto di Astrofisica Spaziale e Fisica Cosmica (IASF-INAF), Via P. Gobetti 101, 40129 Bologna, Italy*

³*School of Physics and Astronomy, University of Southampton, Southampton, SO17 1BJ, UK*

⁴*Centro de Astrobiología (CSIC-INTA), PO Box 78, 28691, Villanueva de la Cañada, Madrid, Spain*

⁵*Istituto di Astrofisica Spaziale e Fisica Cosmica (IASF-INAF), Via Bassini 15, 20122 Milano, Italy*

ABSTRACT

Narrow Line Seyfert 1 (NLSy1) galaxies are a peculiar class of type 1 AGN (BLSy1). The X-ray properties of individual objects belonging to this class are often extreme and associated with accretion at high Eddington ratios. Here we present a study on a sample of 14 NLSy1 galaxies selected at hard X-rays (> 20 keV) from the fourth *INTEGRAL*/IBIS catalogue. The 20–100 keV IBIS spectra show hard X-ray photon indices flatly distributed ($\Gamma_{20-100\text{keV}}$ ranging from ~ 1.3 to ~ 3.6) with an average value of $\langle \Gamma_{20-100\text{keV}} \rangle = 2.3 \pm 0.7$, compatible with a sample of hard X-ray BLSy1 average slope. Instead, NLSy1 show steeper spectral indices with respect to BLSy1 when broad-band spectra are considered. Indeed, we combine XMM-*Newton* and *Swift*/XRT with *INTEGRAL*/IBIS data sets to obtain a wide energy spectral coverage (0.3–100 keV). A constraint on the high energy cut-off and on the reflection component is achieved only in one source, Swift J2127.4+5654 ($E_{\text{cut-off}} \sim 50$ keV, $R = 1.0^{+0.5}_{-0.4}$). Hard X-ray selected NLSy1 do not display particularly strong soft excess emission, while absorption fully or partially covering the continuum is often measured as well as Fe line emission features. Variability is a common trait in this sample, both at X-ray and at hard X-rays. The fraction of NLSy1 in the hard X-ray sky is likely to be $\sim 15\%$, in agreement with estimates derived in optically selected NLSy1 samples. We confirm the association of NLSy1 with small black hole masses with a peak at $10^7 M_{\odot}$ in the distribution, however hard X-ray NLSy1 seem to occupy the lower tail of the Eddington ratios distribution of classical NLSy1.

Key words: galaxies: active - galaxies: Seyfert - X-rays: galaxies

1 INTRODUCTION

Narrow Line Seyfert 1 (NLSy1) are AGN with optical spectral properties similar to those of Seyfert 1 galaxies (Broad Line Seyfert 1, BLSy1), except for having narrow Balmer lines and strong optical FeII lines (Osterbrock & Pogge 1985). The classical definition of NLSy1 (Goodrich 1989) relies on three simple criteria: (i) the full width half maximum (FWHM) of the H_{β} line $< 2000 \text{ km s}^{-1}$; (ii) the $[\text{OIII}] \lambda 5007/H_{\beta}$ ratio < 3 ; and (iii) unusually strong FeII. The NLSy1 and BLSy1 classes are not completely distinct, for

instance Véron-Cetty & Véron (2006) noticed a continuity between their optical spectral properties.

The most extreme characteristics of NLSy1 are seen in the X-ray domain (Gallo 2006). A strong and variable soft excess emission below ~ 1 keV (George et al. 2000, Boller et al. 1996, Turner et al. 1999) is more frequently present than in BLSy1 (Leighly 1999). The 2–10 keV spectral slope is usually steeper in NLSy1 with respect to BLSy1 (Leighly 1999, Brandt et al. 1997) and a sharp spectral drop at about 7 keV has been observed in some objects (Uttley et al. 2004, Longinotti et al. 2003, Boller et al. 2003, Boller et al. 2002). The complex NLSy1 X-ray spectrum has been explained in terms of relativistic blurred disc reflection (e.g., Fabian et al. 2004) or ionized or neutral absorption either totally or partially covering the X-ray source (e.g., Gierliński & Done 2004, Tanaka et al. 2004).

^{*} Based on observations obtained with *INTEGRAL*/IBIS, XMM-*Newton* and *Swift*/XRT

[†] E-mail: francesca.panessa@iasf-roma.inaf.it

Table 1. The hard X-ray selected sample of Narrow Line Seyfert 1 galaxies

Name (1)	RA (2)	DEC (3)	z (4)	H β (5)	[OIII]/H β (6)	[FeII]/H β (7)	N $_{H,Gal}$ (8)	M $_{BH}$ (9)	Ref (10)	S $_R$ (11)	Ref (12)
1H 0323+342	03 24 41.2	+34 10 46	0.0610	1650	~ 0.12	2.0	14.5	7.0	1	362	1
NGC 4051	12 03 09.6	+44 31 53	0.0023	1120	0.55	0.25	1.30	0.17	2,3	9.4	2
Mrk 766	12 18 26.5	+29 48 46	0.0129	1630	1.83	0.35	1.70	0.43	2,4	20.5	2
NGC 4748	12 52 12.4	-13 24 53	0.0146	1565	1.34	0.55	3.60	0.42	2,4	6.0	2
Mrk 783	13 02 58.8	+16 24 27	0.0672	1655	2.29	<0.5	2.00	1.43	2,4	32.9	3
NGC 5506	14 13 14.9	-03 12 27	0.0061	-	7.5	-	3.81	0.2	5,6	227.2	2
IGR J14552-5133	14 55 17.8	-51 34 17	0.0160	1700	0.70 \pm 0.06	≤ 1.70	33.7	0.2	7	-	-
IRAS 15091-2107	15 11 59.8	-21 19 02	0.0446	1480	1.0	0.70	8.40	1.0	8	12.0	4
IGR J16185-5928	16 18 25.7	-59 26 46	0.0350	4000	0.20 \pm 0.03	0.70 \pm 0.06	24.7	2.8	7	-	-
IGR J16385-2057	16 38 30.9	-20 55 25	0.0269	1700	0.50 \pm 0.06	1.20 \pm 0.20	12.0	0.7	9	6.8	3
IGR J16426+6536	16 43 04.1	+65 32 51	0.3230	2100	0.41 \pm 0.04	0.85	3.00	1.1	10	-	-
IGR J19378-0617	19 37 39.0	-06 13 06	0.0106	2700	0.52 \pm 0.04	0.89 \pm 0.06	15.0	0.3	11	42.2	3
ESO 399-IG 020	20 06 58.1	-34 32 58	0.0249	2425	-	-	7.10	-	12	8.4	3
Swift J2127.4+5654	21 27 45.6	+56 56 36	0.0140	2000	0.72 \pm 0.05	1.30 \pm 0.20	78.7	1.5	13,14	6.4	3

Notes: (1): Galaxy name; col (2)-(3) Optical position in epoch J2000; (4) Redshift; (5) FWHM of H β (km/s); (6): [OIII]/H β ratio; (7): [FeII]/H β ratio; (8): Galactic column density in units of 10^{20} cm $^{-2}$; (9): Black hole mass in units of 10^7 solar masses; (10): References for optical and black hole mass measurements: (1) Zhou et al. (2007); (2) Véron-Cetty, M.-P., & Véron, P. (2006); (3) Denney et al. (2009); (4) Wang & Lu (2001); (5) Nagar et al. (2002); (6) Nikolaiuk et al. (2009); (7) Masetti et al. (2006); (8) Osterbrock & De Robertis (1985); (9) Masetti et al. (2008); (10) Masetti et al. (2009); (11) Rodríguez-Ardila et al. (2000); (12) Dietrich et al. (2005); (13) Malizia et al. (2008); (14) Halpern 2006. (11): Radio fluxes in mJy; (12): References for radio fluxes: (1) 5 GHz, Becker et al. (1991); (2) 5 GHz, Gallimore et al. (2006); (3) 1.4 GHz, Condon et al. (1998); (4) 5 GHz, Ulvestad et al. (1995).

A possible interpretation for the peculiar observational properties of NLSy1 is that these systems are accreting close to their Eddington limit, suggesting that, compared to their BLSy1 counterparts, they should host smaller black hole masses ($M_{BH} < 10^8 M_{\odot}$), as measured in the majority of the sources (Wandel et al. 1999, Grupe & Mathur 2004, Whalen et al. 2006). Under the assumption that the H β emitting region is gravitationally bounded to the central black hole, small black hole masses help in explaining the narrow emission lines observed in these objects. It has been shown that NLSy1 galaxies seem not to follow the M_{BH} - σ relation (Komossa & Xu 2007, Grupe & Mathur 2004), suggesting that they may be AGNs in their early stage of development, where small black hole masses grow through accretion in already formed bulges with strong implications for the black hole versus galaxy evolution (Grupe & Mathur 2004, Mathur et al. 2001). However, lately, Marconi et al. (2008) suggested that radiation pressure due to ionizing photons could significantly affect virial black hole mass estimates in highly accreting objects such as NLSy1, resulting in an underestimate of their masses.

The interest on NLSy1 has further increased due to the detection of gamma-ray emission from four NLSy1 with *Fermi* (Abdo et al. 2009) suggesting that NLSy1 may also form a powerful radio jet and at the same time be powered by black holes of moderate masses (Yuan et al. 2008).

The hard X-rays is an energy range where NLSy1 have been poorly investigated so far, only studies on sparse objects are available. *BeppoSAX* observations of a small sample of NLSy1 detected hard X-ray emission in only 2 out of 7 sources (Comastri 2000). *Suzaku* is now providing detailed broad-band studies of targeted NLSy1 (e.g., Ponti et al. 2010, Miniutti et al. 2009, Terashima et al. 2009). Recent hard X-ray surveys performed by the IBIS instrument

(Ubertini et al. 2003) on board *INTEGRAL* (Winkler et al. 2003) and the Burst Alert Telescope (BAT, Barthelmy et al. 2005) on board *Swift* (Geherls et al. 2004) are imaging the hard X-ray sky providing a number of sources detected for the first time at these energies with half of them being newly discovered (Malizia et al. 2010, Landi et al. 2010, Tueller et al. 2010, Tueller et al. 2009, Ajello et al. 2008, Winter et al. 2008, Bassani et al. 2006).

Indeed, the fourth IBIS survey (Bird et al. 2010) has allowed the detection of more than 700 hard X-ray sources over the whole sky above 20 keV, down to an average flux level of about 1 mCrab and with positional accuracies ranging between 0.2 and ~ 5 arcmin, depending on the source strength. Among the detected AGN by IBIS, a small sample of NLSy1 is identified. A first analysis of the hard X-ray properties of a sample of five NLSy1 listed in the third IBIS catalogue (Bird et al. 2007) has been presented in Malizia et al. (2008), combining *Swift*/XRT (X-ray Telescope, Burrows et al. 2005) and *INTEGRAL*/IBIS spectra.

In this work, we present the broad-band X-ray properties of a sample of 14 NLSy1 detected by *INTEGRAL* and present in the fourth IBIS catalogue (Bird et al. 2010). New XMM-*Newton* datasets for 5 NLSy1 of the sample have been combined with *INTEGRAL* data to obtain a wide energy spectrum up to ~ 100 keV. In 5 other objects, XRT data are available below 10 keV, and, for IGR J16426+6536, only an XRT detection is available. Published best-fit spectral parameters for NGC 4051, Mrk 766 and NGC 5506 were taken from the most recent X-ray dedicated works (Terashima et al. 2009, Turner et al. 2007 and Guainazzi et al. 2010, respectively).

The paper is organized in the following manner: Section 2 describes the sample; in Section 3 the observation and data reduction procedure of the *INTEGRAL*, XMM-

Newton and XRT datasets is reported; Section 4 illustrates the broad-band XMM-*Newton* and *INTEGRAL* spectral fitting results; Section 5 is devoted to the discussion of the fraction of NLSy1 in hard X-ray samples and of the black hole mass, Eddington ratios and radio loudness distributions. Finally, in Section 6 we report our conclusions. Throughout this paper we assume a flat Λ CDM cosmology with $(\Omega_M, \Omega_\Lambda) = (0.3, 0.7)$ and a Hubble constant of $70 \text{ km s}^{-1} \text{ Mpc}^{-1}$ (Bennett et al. 2003).

2 THE NARROW LINE SEYFERT 1 SAMPLE

In Table 1 we present the sample of 14 hard X-ray selected NLSy1 from the fourth IBIS/ISGRI soft gamma-ray survey catalog (see Bird et al. 2010 for a complete description of hard X-ray source detection and identification). In the following, we discuss our check on the optical classification for each source. 1H 0323+342 has been classified as a NLSy1 by Zhou et al. (2007), reporting strong optical Fe II complexes. From a multiwavelength study, this object shows the dual properties of both a NLSy1 and a blazar. Indeed, it has been recently detected by the *Fermi*/LAT instrument (Abdo et al. 2009). The optical spectral data of NGC 4051, Mrk 766, NGC 4748 and Mrk 783 have been taken from Véron-Cetty & Véron (2006) (see this work for detailed references on each source). NGC 5506 is reported as a type 1.9 Seyfert galaxy in Bird et al. (2010), however its optical classification has been largely debated. Nagar et al. (2002) proposed a NLSy1 classification based on the permitted OI line (with FWHM $< 2000 \text{ km s}^{-1}$) and on the $1 \mu\text{m}$ Fe II line observed between $0.9\text{--}1.4 \mu\text{m}$. The optical classification of IGR J14552-5133, IGR J16185-5928, IGR J16385-2057, IGR J19378-0617 and SWIFT J2127.4+5654 has been extensively discussed in Malizia et al. (2008) where the relative references are reported¹.

The optical classification of NLSy1 is not always straightforward. Sulentic et al. (2000) and, lately Veron et al. (2006), pointed out that many AGN with $H_\beta > 2000 \text{ km s}^{-1}$ behave like NLSy1 (e.g., strong FeII, strong and variable soft X-ray excess, etc.) and have identified the ratio $\text{FeII}/H_\beta > 0.5$ as a more appropriate dividing line between BLSy1 and NLSy1. This is the case of IGR J16185-5928 and IGR J19378-0617 with $H_\beta > 2000 \text{ km s}^{-1}$ but classified as NLSy1 based on their $[\text{OIII}] \lambda 5007/H_\beta$ and FeII/H_β ratios. Also in ESO 399-IG 020, the H_β FWHM is slightly above 2000 km/s and the source was originally reported as a type 1 Seyfert in Zhou & Wang (2002); lately the source has been reclassified as NLSy1 by Dietrich et al. (2005) (although the authors do not report emission line ratios but only the H_β FWHM and its flux, i.e., $1.2 \times 10^{-13} \text{ ergs cm}^{-2} \text{ s}^{-1}$). In Osterbrock & De Robertis (1985), IRAS 15091-2107 is classified as a type 1 Seyfert, notwithstanding that the HI emission lines are only slightly broader than the forbidden lines

and FeII emission is as strong as observed in NLSy1. Subsequently, Goodrich (1989) classified this source as a NLSy1. The classification as a NLSy1 for IGR J16426+6536 is given in Masetti et al. (2009), while Butler et al. (2009) classified IGR J16426+6536 as a Seyfert 1.5. However, the two observations were separated by several months suggesting possible intrinsic variability.

References to black hole mass estimates are reported in Table 1, all of them were calculated through the radius-luminosity relation as in Kaspi et al. (2000). In Table 1, we also report radio fluxes in mJy and their relative references.

3 OBSERVATIONS AND DATA REDUCTION

3.1 The INTEGRAL data

The *INTEGRAL*/IBIS data used in this work have been collected in the 4th IBIS survey (Bird et al. 2010) consisting of 7355 pointings (called Science Windows, ScW, lasting about 2000 sec each) performed from the beginning of the Mission in November 2002 up to April 2008 and including both all available public and Core Programme data. IBIS/ISGRI images for each available pointing were generated in various energy bands using the ISDC off-line scientific analysis software OSA (Goldwurm et al. 2003). Then all images have been mosaicked to create significance map at revolution level (each orbit lasting about 3 days) and for all the available pointings. Count rates at the position of the source were extracted from individual images in order to provide light curves in various energy bands; from these light curves, average fluxes were then extracted and combined to produce an average source spectrum (see Bird et al. 2010 for details).

A spectral fit with a simple power-law model has been performed using the IBIS spectra. In Table 2 we report the source significance, the total on-source exposure, the map code as from Bird et al. (2010), indicating the best significance energy band, the hard X-ray photon index, the fit chi-squared over degrees of freedom ratio, the 20-100 keV flux and luminosity. We also report the 20-100 keV flux from the *Swift*/BAT 54 months catalogue, estimated from the averaged 14-150 keV fluxes listed in Cusumano et al. (2010), assuming $\Gamma = 2$.

3.2 The XMM-Newton data

In Table 3 the log of XMM-*Newton* observations is listed. The software SASv9.0 has been used for the data reduction procedure. In many cases, observations were heavily affected from high-background flares, therefore data were cleaned through an inspection of the high energy light curves, effective exposures obtained after screening are those listed in Table 3. The source spectra and light curves were extracted from circular regions centered on the sources while background circular regions were chosen to be free from contaminating sources. The *arfgen* and *rmfgen* SAS tasks were used to create ancillary and response files. The number of counts per channel were chosen depending on the source photon statistics. For the sake of simplicity we discuss data of the EPIC pn cameras only, while the MOS1 and MOS2 spectra have been checked for consistency.

¹ These sources have been classified during the optical follow-up campaigns which are on-going to identify the *INTEGRAL*/IBIS sources (Masetti et al. 2010 and references therein). See the web page <http://www.iasfbo.inaf.it/extras/IGR/main.html> for the information about the *INTEGRAL* sources identified using optical or near-infrared (NIR) observations.

Table 2. The hard X-ray data

Name (1)	Significance (2)	Exposure (3)	Map Code (4)	$\Gamma_{20-100\text{keV}}$ (5)	χ^2/dof (6)	$F_{20-100\text{keV}}$ (7)	$L_{20-100\text{keV}}$ (8)	$F_{\text{Swift}/\text{BAT}}$ (9)
1H 0323+342	6.8	128	18-60	$1.55^{+0.80}_{-1.20}$	1.28/5	5.3	44.67	1.7
NGC 4051	10.0	528	20-40	$2.16^{+0.41}_{-0.38}$	7.59/8	3.6	41.62	2.3
Mrk 766	7.1	584	20-40	$2.85^{+0.85}_{-0.68}$	6.00/7	2.0	42.88	1.3
NGC 4748	5.2	841	18-60	$1.43^{+0.92}_{-1.05}$	9.05/7	1.7	42.91	0.6
Mrk 783	5.8	626	20-100	$3.62^{+2.00}_{-1.54}$	3.21/7	0.8	43.97	1.1
NGC 5506	9.0	25.1	18-60	$2.41^{+0.68}_{-0.59}$	7.64/6	16.1	43.12	14.8
IGR J14552-5133	8.8	2558	18-60	$1.90^{+0.44}_{-0.46}$	5.40/8	1.5	42.93	1.3
IRAS 15091-2107	4.5	258	20-40	$2.95^{+1.13}_{-0.92}$	2.59/9	1.8	43.94	—
IGR J16185-5928	8.5	2213	18-60	$1.34^{+0.82}_{-0.40}$	3.26/8	1.7	43.69	1.0
IGR J16385-2057	5.5	1066	20-100	$3.07^{+1.00}_{-0.71}$	5.47/6	1.4	43.38	1.3
IGR J16426+6536	6.2	97	18-60	$3.34^{+1.98}_{-1.57}$	2.07/5	2.5	46.10	—
IGR J19378-0617	6.1	727	20-100	$2.14^{+0.65}_{-0.56}$	18.66/10	1.8	42.66	1.4
ESO 399-IG 020	5.5	932	20-100	$1.54^{+0.63}_{-0.58}$	1.90/8	1.7	43.39	1.3
Swift J2127.4+5654	19.4	1781	18-60	$2.50^{+0.24}_{-0.24}$	7.21/7	3.4	43.17	2.2

Notes: (1): Galaxy name; (2): Maximum source significance in the map; (3): On-source exposure (ks); (4): Energy range with source maximum significance; (5): hard X-ray photon index; (6): Chi squared and degree of freedom ratio; (7): 20-100 keV *INTEGRAL*/IBIS flux in 10^{-11} ergs cm^{-2} s^{-1} ; (8): Logarithm of 20-100 keV *INTEGRAL*/IBIS luminosity in ergs s^{-1} ; (9): 20-100 keV *Swift*/BAT flux in 10^{-11} ergs cm^{-2} s^{-1} adapted from Cusumano et al. (2010).

Table 3. XMM-Newton and Swift/XRT Data Observation Details

Name (1)	Instrument (2)	Obs. Date (3)	Exposure (4)	Filter (5)
1H 0323+342	XRT	2006-07-05	8071	—
	XRT	2006-07-09	8802	—
	XRT	2007-11-04	1885	—
IRAS 15091-2107	XMM	2005-07-26	9305	medium
NGC4748	XRT	2005-12-28	2243	—
	XRT	2007-01-09	2266	—
Mrk 783	XRT	2008-05-09	6305	—
	XRT	2008-08-16	4487	—
IGR J14552-5133	XRT	2006-12-27	3728	—
	XRT	2007-01-02	4695	—
IGR J16185-5928	XMM	2009-02-18	8402	thin
IGR J16385-2057	XMM	2009-03-15	7807	medium
	XMM	2010-02-15	19800	medium
IGR J19378-0617	XMM	2009-04-28	12240	thin
ESO 399-IG 020	XRT	2010-08-27	8361	—
Swift J2127.4+5654	XMM	2009-11-11	8631	thin

Notes: (1): Galaxy name; (2): Instrument; (3): Observation date; (4): pn observation exposures in sec; (5): pn filters.

In Figure 1 we show the XMM-Newton light curves (binning time of 100 s) between 0.3-2 keV (top panel), 2-10 keV (middle panel) and the hardness ratio (2-10 keV/0.3-2 keV) (bottom panel) for each source. In Table 4 we report the χ^2/dof obtained by fitting the light curves and hardness ratios with a constant; we have marked in bold face the χ^2/dof with variability at less than 3 sigma confidence level. It is clear that, in both energy ranges, the short term light curves show significant variability, in 50% of the cases; the soft flux is more variable than the 2-10 keV flux, as expected in NLSy1. The only exceptions are IRAS 15091-2107 and IGR J16185-5928, where the 2-10 keV flux is more variable than the soft flux. The hardness ratios reflect some evidence of spectral variability, although this is more prominent only in

IGR J19378-0617 and indeed, this issue is investigated in details in a dedicated *Suzaku* observation (Miniutti et al. in preparation). Given the variable nature of NLSy1 a time-resolved spectral analysis would be advisable, however the XMM-Newton and XRT exposures are too short for a statistically significant analysis, therefore we extract the spectra from the total light curves.

With the aim of deriving the optical-to-X-ray spectral slope α_{ox} ², optical U and UVW1 fluxes were extracted using the Optical Monitor (OM, Mason et al. 2001) data, already available from the XMM-Newton pipeline products.

² $\alpha_{ox} = -0.384 \log(f_{2\text{keV}}/f_{2500\text{\AA}})$, Tananbaum et al. (1979)

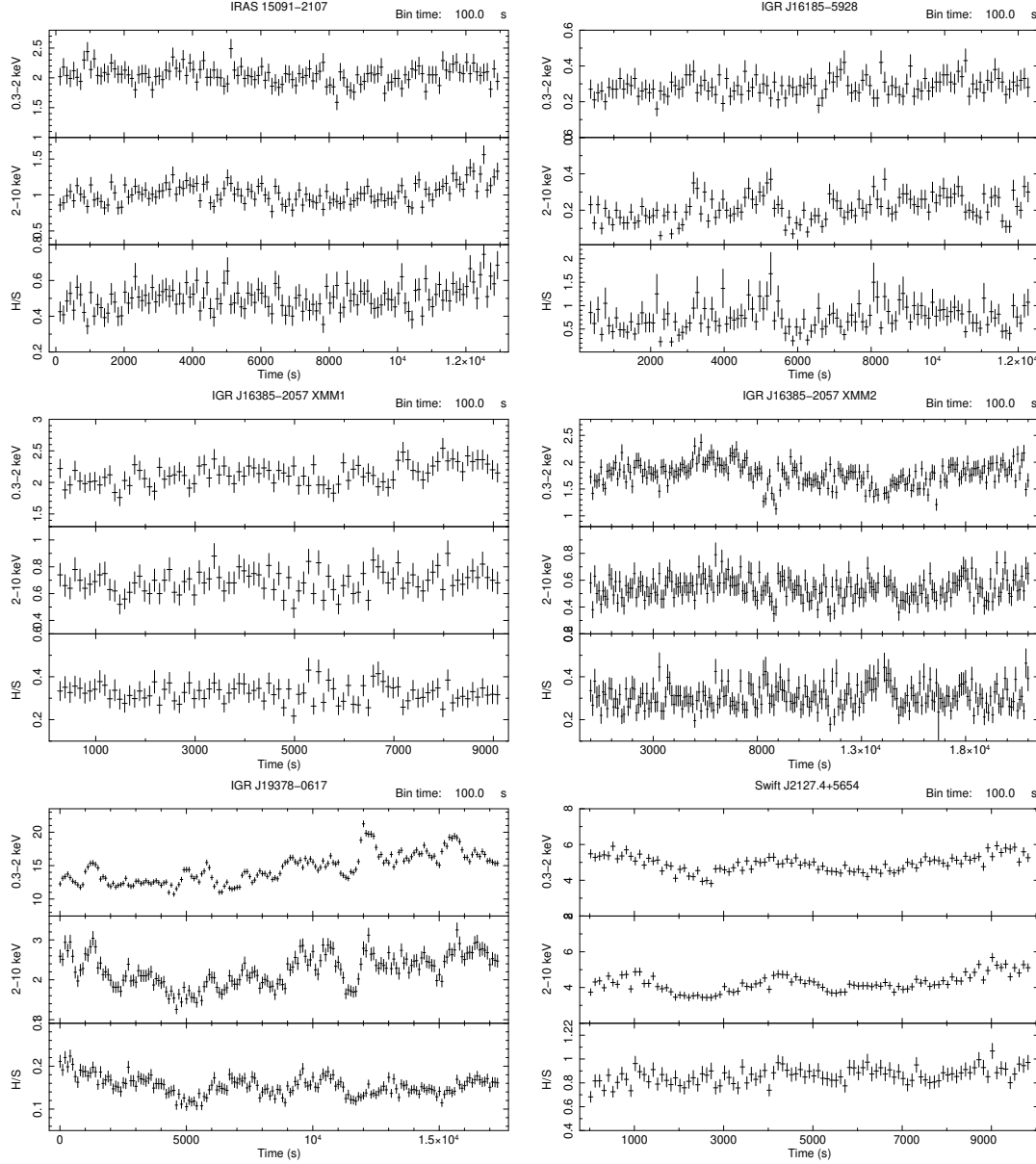


Figure 1. XMM-Newton light curves

Table 4. XMM-Newton light curve analysis.

Name (1)	Count rate (0.3-2 keV) (2)	χ^2/dof (3)	Count rate (2-10 keV) (4)	χ^2/dof (5)	Hardness ratio (6)	χ^2/dof (7)
IRAS 15091-2107	2.03 ± 0.02	130/129	1.01 ± 0.01	226/129	0.49 ± 0.02	162/129
IGR J16185-5928	0.28 ± 0.01	106/120	0.18 ± 0.01	324/120	0.61 ± 0.02	190/120
IGR J16385-2057 XMM1	2.12 ± 0.02	107/89	0.68 ± 0.01	91/89	0.32 ± 0.01	77/89
IGR J16385-2057 XMM2	1.67 ± 0.02	1954/209	0.49 ± 0.01	817/209	0.29 ± 0.01	254/209
IGR J19378-0617	14.25 ± 0.05	5421/174	2.16 ± 0.02	1335/174	0.15 ± 0.01	662/174
Swift J2127.4+5654	4.89 ± 0.03	401/99	4.18 ± 0.03	532/99	0.85 ± 0.02	138/99

Note: (1): Galaxy name; (2): Count rate (counts s^{-1}) in the 0.3-2 keV band; (3): Chi-squared and degrees of freedom from fitting the 0.3-2 keV light curve with a constant; (4): Count rate (counts s^{-1}) in the 2-10 keV band; (5): Chi-squared and degrees of freedom from fitting the 2-10 keV light curve with a constant. (6): Hardness ratio (2-10 keV/0.3-2 keV); (7): Chi-squared and degrees of freedom from fitting the hardness ratio. In bold face the χ^2/dof with variability at less than 3 sigma confidence level are marked.

The background subtracted net count rates were converted into fluxes by applying the OM count conversion factors. Finally a correction for Galactic reddening was applied using the E_{B-V} values by Schlegel et al. (1998) and using the standard reddening correction curves by Cardelli et al. (1989). In Table 5 details of the OM data are reported.

3.3 The *Swift*/XRT data

For five sources in our sample, we also have X-ray observations acquired with the XRT on board the *Swift* satellite. XRT data reduction was performed using the XRTDAS standard data pipeline package (XRTPIPELINE v. 0.12.4), in order to produce screened event files. All data were extracted only in the Photon Counting (PC) mode (Hill et al. 2004), adopting the standard grade filtering (0–12 for PC) according to the XRT nomenclature. Events for spectral analysis were extracted within a circular region of radius $47''$ (corresponding to 20 XRT pixels), centered on the source position, which encloses about 90% of the PSF at 1.5 keV (see Moretti et al. 2004). The background was taken from various source-free regions close to the X-ray source of interest, using circular regions with different radii in order to ensure an evenly sampled background. In all cases, the spectra were extracted from the corresponding event files using the XSELECT software and binned to 20 counts per bin using GRPPHA, so that the χ^2 statistic could be applied. We used version v.011 of the response matrices and create individual ancillary response files *arf* using XRTMKARF v.0.5.6.

1H 0323+342, NGC 4748, Mrk 783 and IGR J14552-5133 have multiple observations with XRT and, to increase the spectral statistics, we fit the data sets together, tying the different parameters only in case of no or little variability. The strongest flux variation is observed in the blazar-like NLSy1 1H 0323+342, where its flux has increased by a factor of ~ 10 after two days. Unfortunately, the *INTEGRAL* observations were performed between July and August 2004 and therefore, are not simultaneous with XRT data (see also Foschini et al. 2009, for a presentation of the X-ray and hard X-ray behaviour of this source). In NGC 4748, no spectral variation is found between the two ~ 2 ks XRT observations, therefore we tie the XRT photon indices to the same value in the fitting procedure and report in Table 6 the fluxes and cross-calibration constants. In Mrk 783, the two XRT observations present both flux and spectral variability, while neutral absorption is significantly required only in the first observation. Only little spectral and flux variation is found in IGR J14552-5133.

We have estimated the 2500 Å flux using data from the UVW1 filter of the UV/Optical Telescope (UVOT, Roming et al. 2005) onboard *Swift*. From each segment data were co-added by the UVOT task *uvotimsum*. A circle of $3''$ radius centered on the source has been used to extract source counts, taking into account the aperture correction. An annular background region centered on the source is used, with an inner radius of $27.5''$ and a width of $7.5''$, except for IGR J14552-5133 for which an off-source circle (with a radius of $15''$) was used to avoid contamination from nearby sources. The data were analyzed with the UVOT software tool *uvotsource*, using the count rate to flux/magnitude conversion as in Poole et al. (2008). Magnitudes were corrected for Galactic reddening using the E_{B-V} values by Schlegel

et al. (1998) and using the standard reddening correction curves by Cardelli et al. (1989). In Table 5 we report the UVOT data log. Given the extreme variability between the three XRT observations of 1H 0323+342, we report the three simultaneous UVOT/XRT α_{ox} .

3.4 Broad-band spectral analysis

Since the XMM-Newton/XRT and *INTEGRAL* observations are not simultaneous, a cross-calibration constant C is left free to vary to take into account possible cross-calibration mismatches between the two instruments but more importantly in these objects, to consider variability effects. The cross-calibration constants between *INTEGRAL* and XMM-Newton, XRT and *Chandra* have been typically found narrowly distributed around unity using various source typologies (e.g. Molina et al. 2009, De Rosa et al. 2008; Masetti et al. 2007; Panessa et al. 2008), thus suggesting that significant deviation from this value is confidently attributed to source flux variations.

With the aim of characterizing broadly the spectral properties of the sample, we have added extra components to a baseline model composed of a simple power-law with absorption fixed at the Galactic value, to model spectral residuals.

Both an emission line spectrum from hot diffuse gas (*MEKAL* in Xspec) and/or a disk black body component (*DISKBB* in Xspec) has been tested to model the soft X-ray emission; in more complex spectra, absorption edges were added with energies ranging from 0.7 to 2 keV, as expected from a "warm" absorber (Reynolds 1997).

Residuals around 6-7 keV have been modeled with one or two gaussian components representing the Fe line neutral/ionized transitions. Whenever necessary, the curvature of the continuum was modeled with a partial covering absorption. The cut-off power-law and *peaxrav* models were tested on each source. However, the best-fit model for all the sources in the sample is achieved by using a simple power-law model, except for Swift J2127.4+5654 for which a *peaxrav* model better represents data. The spectral fitting results are reported in Table 6 and broad-band spectra are shown in Figure 2 and 3. Spectral best fitting was performed using XSPEC v12.5.0 (Arnaud 1996). The quoted errors on the model parameters correspond to a 90% confidence level for one interesting parameter.

The broad-band spectrum for three sources of our sample (i.e., NGC 4051, Mrk 766 and NGC 5506) has previously been studied in the literature (Terashima et al. 2009, Turner et al. 2007 and Guainazzi et al. 2010, respectively). For the purpose of a general broad-band statistical analysis of the total sample, we have used the best-fit spectral parameters reported in literature for these three sources, using the averaged spectral values and fluxes. Similarly, for the sources analyzed in this work having multiple observations, we have used the averaged parameters in our plots.

Table 5. XMM-Newton Optical Monitor and Swift/UVOT Data

Name (1)	Instrument (2)	Obs. Date (3)	Filter (4)	E(B - V) (5)	Optical Flux (6)	α_{ox} (7)
1H 0323+342	XRT	2006-07-05	UVW1	0.213	2.83 \pm 0.21	1.6
	XRT	2006-07-09	UVW1		2.94 \pm 0.22	1.2
	XRT	2007-11-04	UVW1		1.74 \pm 0.14	1.3
NGC4748	XRT	2007-01-09	UVW1	0.052	3.08 \pm 0.23	1.4
Mrk 783	XRT	2008-08-16	UVW1	0.028	1.15 \pm 0.08	1.2
IGR J14552-5133	XRT	2006-12-27	UVW1	0.662	4.69 \pm 0.48	1.4
IRAS 15091-2107	XMM	2005-07-26	UVW1	0.118	0.18 \pm 0.01	0.9
IGR J16185-5928	XMM	2009-02-18	U	0.322	0.22 \pm 0.01	1.1
IGR J19378-0617	XMM	2009-04-28	U	0.293	2.72 \pm 0.03	1.1
ESO 399-IG 020	XRT	2010-08-27	UVW1	0.113	0.98 \pm 0.08	1.5
Swift J2127.4+5654	XMM	2009-11-11	UVW1	1.298	294.0 \pm 18.9	1.8

Notes: (1): Galaxy name; (2): Instrument; (3): Observation date; (4): OM/UVOT filter; (5): (5): Optical flux in units of 10^{-11} erg $\text{cm}^{-2} \text{s}^{-1}$; (6): Optical-to-X-ray slope α_{ox} .

Table 6. Combined XMM-Newton/XRT and INTEGRAL continuum spectral analysis

Name (1)	$N_{H,int}$ (2)	Cvr (3)	$\Gamma_{0.3-100\text{keV}}$ (4)	C (5)	F _{0.1-2} (6)	F ₂₋₁₀ (7)	L _{0.1-2} (8)	L ₂₋₁₀ (9)	χ^2/dof (10)
1H 0323+342 XRT1	—	—	1.98 $^{+0.16}_{-0.09}$	6.70 $^{+0.82}_{-0.66}$	0.15	0.18	43.06	43.14	246/205
1H 0323+342 XRT2	—	—	2.05 $^{+0.05}_{-0.05}$	3.50 $^{+0.54}_{-0.45}$	0.77	1.11	43.77	43.93	246/205
1H 0323+342 XRT3	—	—	1.99 $^{+0.13}_{-0.12}$	24.9 $^{+21.2}_{-11.4}$	0.40	0.64	43.49	43.69	246/205
NGC 4748 XRT1	—	—	2.01 $^{+0.13}_{-0.13}$	1.47 $^{+0.20}_{-0.18}$	0.35	0.34	42.19	42.18	40/41
NGC 4748 XRT2	—	—	2.01 $^{+0.13}_{-0.13}$	>0.37	0.52	0.50	42.36	42.35	40/41
Mrk 783 XRT1	0.15 $^{+0.09}_{-0.08}$	—	1.75 $^{+0.23}_{-0.22}$	1.88 $^{+0.64}_{-0.40}$	0.30	0.41	43.45	43.59	81/80
Mrk 783 XRT2	> 0.11	—	1.65 $^{+0.17}_{-0.15}$	2.09 $^{+2.09}_{-1.11}$	0.41	0.89	43.59	43.92	81/80
IGR J14552-5133 XRT1	—	—	1.91 $^{+0.10}_{-0.10}$	1.08 $^{+0.15}_{-0.12}$	0.33	0.96	42.24	42.71	72/89
IGR J14552-5133 XRT2	—	—	2.11 $^{+0.10}_{-0.10}$	1.19 $^{+0.48}_{-0.34}$	0.34	0.77	42.26	42.61	72/89
IRAS 15091-2107	0.14 $^{+0.04}_{-0.04}$	0.75 $^{+0.04}_{-0.04}$	1.75 $^{+0.04}_{-0.03}$	1.54 $^{+0.56}_{-0.50}$	0.47	0.90	43.29	43.57	431/480
IGR J16185-5928	10.6 $^{+16.0}_{-5.5}$	0.47 $^{+0.19}_{-0.18}$	2.00 $^{+0.09}_{-0.09}$	6.23 $^{+2.80}_{-2.68}$	0.13	0.27	42.52	42.84	185/212
IGR J16385-2057 XMM1	—	—	1.50 $^{+0.05}_{-0.07}$	0.60 $^{+0.21}_{-0.18}$	0.40	0.70	42.78	43.02	593/606
IGR J16385-2057 XMM2	—	—	1.84 $^{+0.06}_{-0.06}$	1.64 $^{+0.51}_{-0.46}$	0.32	0.53	42.68	42.90	595/551
IGR J19378-0617	32.0 $^{+10.5}_{-8.0}$	0.47 $^{+0.05}_{-0.05}$	2.58 $^{+0.02}_{-0.02}$	1.37 $^{+0.40}_{-0.35}$	3.4	2.7	42.90	42.80	487/465
ESO 399-IG 020	—	—	1.69 $^{+0.17}_{-0.17}$	>0.80	0.07	0.13	41.95	42.22	19/22
Swift J2127.4+5654	—	—	1.94 $^{+0.07}_{-0.08}$	0.84 $^{+0.21}_{-0.17}$	1.0	4.2	42.61	43.23	1337/1265*

Note: (1): Galaxy name; (2): Intrinsic fully or partially covering column density in units of 10^{22} cm^{-2} ; (3): Covering factor; (4) Power-law photon index; (5): Value of the XMM-Newton/INTEGRAL and XRT/INTEGRAL cross-calibration constant; (6-7): Model unabsorbed fluxes in the 0.1-2 keV and 2-10 keV bands in units of $10^{-11} \text{ erg cm}^{-2} \text{s}^{-1}$; (8-9): Logarithm of the unabsorbed luminosities in the 0.1-2 keV and 2-10 keV bands; (10): Chi-squared and degrees of freedom. * Best fit obtain with a *pearrv* model and the addition of an extra gaussian component at 5.8 keV (see Section 4.2).

Table 7. Fe lines and soft excess spectral analysis.

Name (1)	E_{α} (2)	σ (3)	EW_{α} (4)	E_{α} (5)	σ (6)	EW_{α} (7)	kT (8)	kT_{in} (9)	χ^2/dof (10)
IRAS 15091-2107	6.31 $^{+0.14}_{-0.10}$	0.19 $^{+0.26}_{-0.07}$	170 $^{+150}_{-60}$	—	—	—	—	—	431/480
IGR J16385-2057 XMM1	6.37 $^{+0.07}_{-0.18}$	0.01 fix	71 $^{+47}_{-47}$	—	—	—	0.60 $^{+0.09}_{-0.13}$	0.48 $^{+0.03}_{-0.03}$	593/606
IGR J16385-2057 XMM2	6.60 $^{+0.06}_{-0.06}$	0.01 fix	75 $^{+38}_{-38}$	6.97 $^{+0.04}_{-0.05}$	0.01 fix	90 $^{+33}_{-26}$	0.13 $^{+0.03}_{-0.03}$	0.33 $^{+0.03}_{-0.03}$	595/551
IGR J19378-0617	—	—	—	—	—	—	0.22 $^{+0.01}_{-0.01}$	—	487/465
Swift J2127.4+5654	6.40 $^{+0.04}_{-0.04}$	0.01 fix	46 $^{+14}_{-14}$	5.80 $^{+0.04}_{-0.04}$	0.01 fix	38 $^{+22}_{-20}$	0.22 $^{+0.01}_{-0.01}$	—	1337/1265

Note: (1): Galaxy name; (2): Energy of the Fe line in keV; (3): Line width in keV; (4): Equivalent width of the Fe line in eV; (5): Energy of a second gaussian component in keV; (6): Line width in keV; (7): Equivalent width in eV; (8): Plasma temperature in keV; (9): DISKBB temperature at inner disk radius (keV); (10): Chi-squared and degrees of freedom.

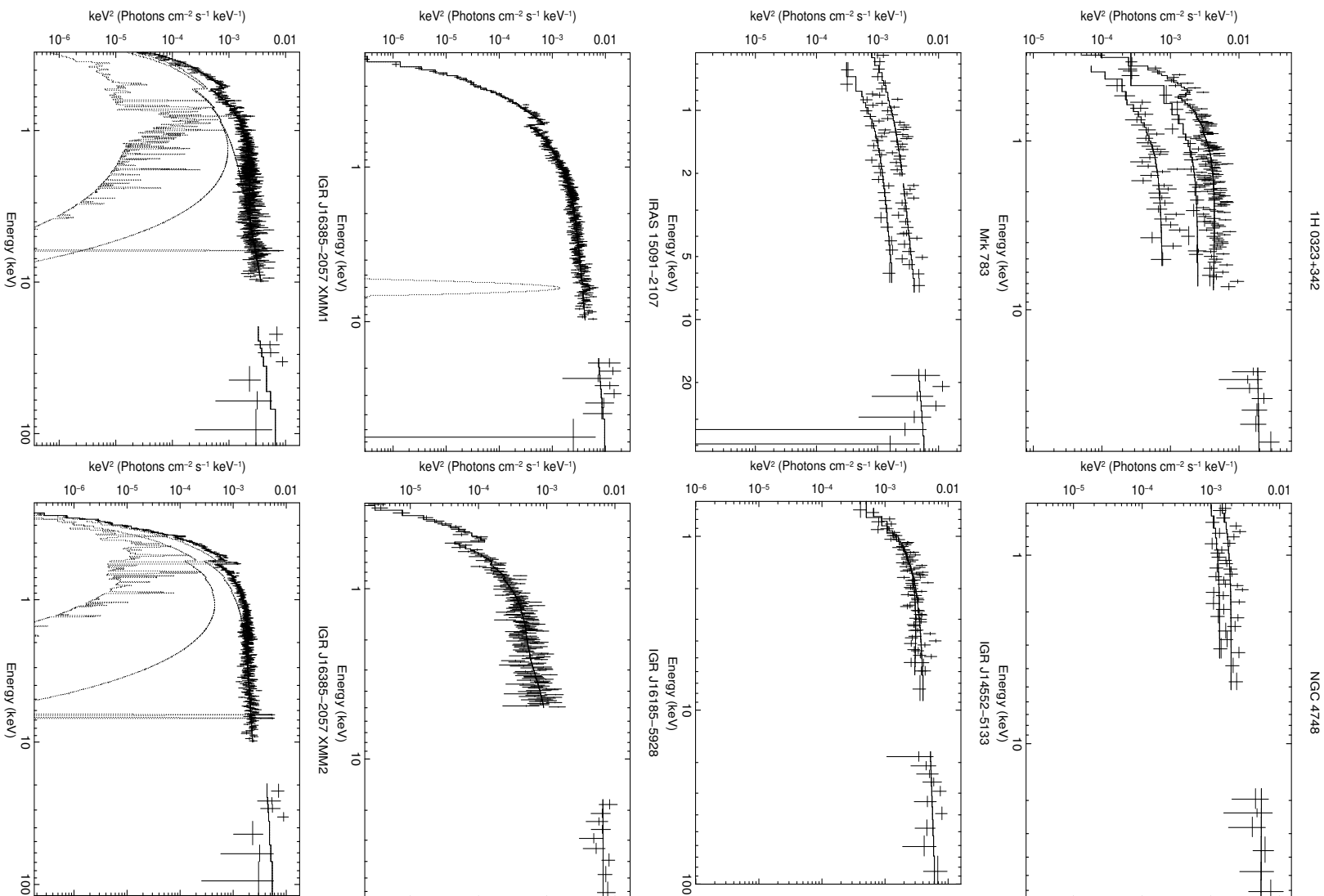


Figure 2. Broad-band XMM-*Newton*/XRT and *INTEGRAL* best-fit spectra.

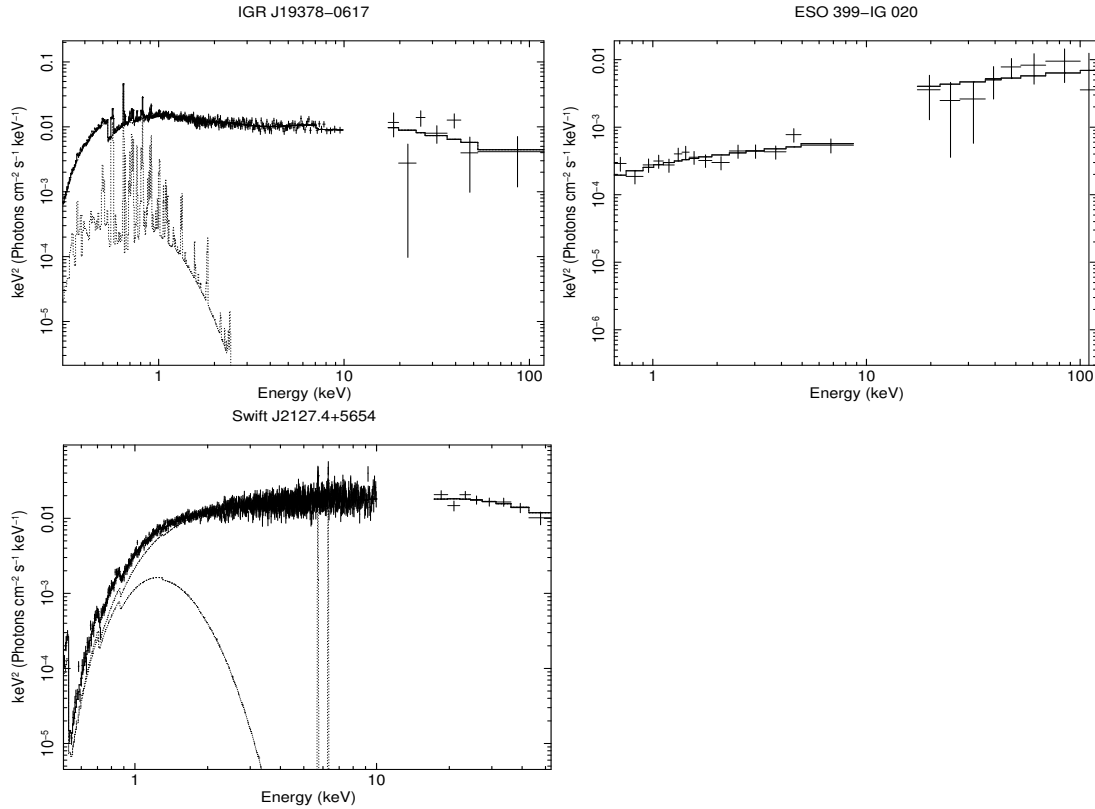


Figure 3. Broad-band XMM-Newton/XRT and *INTEGRAL* best-fit spectra.

4 RESULTS

4.1 Continuum slope and high energy cut-off

In Figure 4 (left panel), the hard photon index distribution in NLSy1 sample (shaded histogram) is compared to the *INTEGRAL* BLSy1 one (IBIS fourth catalogue, Molina et al. in preparation). The hard photon index is broadly distributed in our sample ranging from ~ 1.3 to very steep values such as ~ 3.6 , with a mean value $\langle \Gamma_{20-100\text{keV}} \rangle = 2.3 \pm 0.7$ ³ (see Table 2). This value is consistent within errors with the one previously found in a smaller sample of five *INTEGRAL* NLSy1 ($\langle \Gamma_{20-100\text{keV}} \rangle = 2.6 \pm 0.3$, Malizia et al. 2008). The BLSy1 mean hard photon index ($\langle \Gamma_{20-100\text{keV}} \rangle = 2.0 \pm 0.2$) is only slightly flatter and consistent with the NLSy1 $\langle \Gamma_{20-100\text{keV}} \rangle$, as indeed a Kolmogorov-Smirnov (K-S) test (probability $P = 0.030$ of a random result) indicates that the distributions are not significantly different. This is also in agreement with estimates from type 1 Seyfert spectra from *Swift*/BAT ($\langle \Gamma_{20-100\text{keV}} \rangle = 2.23 \pm 0.11$, Ajello et al. 2008). From this analysis, the average photon index of NLSy1 at hard X-rays appears not to be steeper than in BLSy1, however, we should consider that faint steep spectrum sources may be missed by hard X-ray surveys.

By fitting the 0.3-100 keV broad-band spectrum (as in Table 6 and including data from literature for NGC 4051, Mrk 783 and NGC 5506), the resulting photon index varies

from ~ 1.5 to ~ 2.6 with a mean of $\langle \Gamma_{0.3-100\text{keV}} \rangle = 2.0 \pm 0.3$, consistent with the typical values found for this class of sources (e.g., Leighly 1999). We should note that the 0.3-100 keV spectral fit parameters are more representative of the spectra below 10 keV, for the larger statistics, especially when XMM-Newton data are used. In a complete hard X-ray selected sample of BLSy1, Molina et al. (2009) found a flatter mean value $\langle \Gamma_{20-100\text{keV}} \rangle \sim 1.7$ ($\sigma = 0.2$), confirming the evidence that NLSy1 tend to have steeper photon indices, as also confirmed in Bianchi et al. (2009a), for an X-ray selected sample. Therefore, no clear separation between NLSy1 and BLSy1 average hard X-ray photon index is found as instead observed for the broad-band photon index.

In Figure 4 (right panel) we plot the hard X-ray versus the 0.3-100 keV broad band X-ray photon index. The one-to-one regression line is also drawn. The steeper hard X-ray photon indices are also clear from this plot suggesting the possible presence of a high energy cut-off. However, with the present data we were able to constrain this parameter only in Swift J2127.4+5654 ($E_{\text{cut-off}} = 49^{+49}_{-17}$ keV), in agreement with our previous *INTEGRAL* estimate (Malizia et al. 2008) and with the *Suzaku* PIN measurement (Miniutti et al. 2009). A very steep hard X-ray photon index is measured in Mrk 766 ($\Gamma \sim 2.9$) and indeed, a spectral decrease is evident at ~ 50 keV from the *Suzaku* PIN data (Turner et al. 2007). In Mrk 783, IRAS 15091-2107 and in IGR J16385-2057 the hard X-ray photon index is much steeper than the XRT and XMM-Newton one, however the cut-off energy measured from the broad-band analysis would be phys-

³ We use the arithmetic mean and adopt its standard deviation as a measure of each parameter spread, given the extreme non-Gaussian distribution of the data points.

ically unexpected ($E_{cut-off} \sim 20$ keV). Instead, the XMM-Newton/XRT and *INTEGRAL* mismatch is likely due to spectral and/or flux variability. Finally, IGR J16426+6536 shows a steep hard X-ray photon index, however the lack of data below 10 keV does not allow a constraint on the broad-band spectrum.

4.2 Fe K emission lines and reprocessing features

Fe emission lines are ubiquitously found in Seyfert spectra (e.g., Nandra et al. 1997). Indeed, the origin of both the narrow and broad component is still controversial and NLSy1 often do show complex, variable and multiple components, as in the case of NGC 4051, Mrk766 and NGC 5506 (for a comprehensive report on the Fe line properties see Terashima et al. 2009, Turner et al. 2007 and Guainazzi et al. 2010 respectively).

A fluorescent emission line around 6-7 keV is detected in three out of four NLSy1 observed by XMM-Newton (see Table 7), this fraction increases to six out of seven if we consider the line detections in NGC 4051, Mrk 766 and NGC 5506. We must consider that no data at these energies are available in the IGR J16185-5928 XMM-Newton spectrum since it is dominated by the background, due to high flaring activity in a short exposure observation. The Fe line is not significantly required in the IGR J19378-0617 spectral fitting, although a weak feature is present. In IRAS 15091-2107 the line profile is consistent with a moderately broad Gaussian component, while between the two XMM-Newton observations of IGR J16385-2057 the line has varied its energy; also, marginal evidence for a narrow line at ~ 7 keV ($EW = 60^{+50}_{-40}$ eV) in both observations suggest the presence of variable ionized Fe lines in this source. A broad relativistic Fe line has been detected in a *Suzaku* observation of Swift J2127.4+5654 (Miniutti et al. 2009). Time-resolved spectroscopy performed on a small portion of the light curve when the source is at an higher flux state reveals the presence of two narrow Gaussian line at 5.83 ± 0.12 keV and at 6.57 ± 0.10 keV. We confirm this evidence and significantly detect an emission line at 5.8 keV. A deeper investigation on the line properties of this source is ongoing using a longer (~ 100 ks) XMM-Newton observation (Miniutti et al. in preparation).

Overall, the modeling of the broad-band X-ray spectrum with a cut-off power-law continuum reflected from neutral material (*pe_xrav*) does not provides a significant increase of the fit quality. In the case of IGR J16185-5928, the XMM-Newton and *INTEGRAL* flux difference results in an extremely high reflection value $R = 14.9^{+9.3}_{-7.4}$ (with $C_{pn/IBIS} = 1.4^{+0.6}_{-0.4}$ instead of ~ 6.2 when modeling with a power-law); this is probably to be ascribed to variability as shown from the *Suzaku* longer observation, where a more moderate reflection fraction is measured ($R = 0.9 \pm 0.2$, Miniutti et al. in preparation). The 20-100 keV *Suzaku* flux of 1.5×10^{-11} erg cm $^{-2}$ s $^{-1}$ is consistent with the average *INTEGRAL* flux of 1.7×10^{-11} erg cm $^{-2}$ s $^{-1}$, while during the XMM-Newton observation the 2-10 keV flux was a factor of ~ 3 lower than that of *Suzaku*. The reflection fraction is well constrained in Swift J2127.4+5654 ($R = 1.1^{+0.8}_{-0.7}$) in agreement with the *Suzaku* value ($R = 1.0^{+0.5}_{-0.4}$, Miniutti et al. 2009).

4.3 Soft X-ray components and absorption

The soft X-ray emission is one of the most peculiar characteristics in NLSy1 for its complex shape and variability. In this work, only phenomenological models are used to characterize the soft emission, such as a disk black body model and an emission line spectrum from hot diffuse gas. It has been noticed that the use of a thermal disk model in AGN results in a very narrow range of disk temperatures independently on the range of luminosities and black hole masses spanned (Ponti et al. 2006). Different models involving atomic physics processes could certainly be more adequate to describe the soft X-ray emission (e.g., Gierliński & Done 2004), however this is beyond the scope of this work where a simple representation of the average properties is instead provided.

In our sample, a *MEKAL* model well represents the soft emission in all sources except for IRAS 15091-2107 and IGR J16185-5928 for which no evidence of soft X-ray emission is found. The temperatures are in the range between 0.1 to 0.6 keV. The addition of a black body model is also required in the spectral fitting of IGR J16385-2057, where the temperature varies between the two observations as well as a larger variation is seen in the temperature of the hot plasma, suggestive of spectral variability also at soft energies. The presence of absorption edges due to O VII (0.737 keV) and O VIII (0.871 keV) is not required in the sources spectral fitting.

The most complex and prominent soft spectrum is shown by IGR J19378-0617 where two absorption edges are needed to model the spectral features at 1.23 ± 0.03 keV ($\tau = 0.13 \pm 0.02$) and 1.57 ± 0.03 keV ($\tau = 0.16 \pm 0.03$); such features have been previously detected in AGN and interpreted in terms of highly blue-shifted absorption material, resonance absorption by Fe L (see Leighly 1999), as expected from partially ionized absorption by a warm absorber and/or reflection off the accretion disc.

The presence of strong, partial and/or stratified absorption has also been found in NGC 4051, Mrk 766 and NGC 5506 and is one of the competing models applied in objects with complex spectra. Intrinsic absorption was measured in four sources of the sample, in three objects it partially covers the continuum and in IGR J19378-0617 this value is significantly high ($\sim 3 \times 10^{23}$ cm $^{-2}$), similar to the amount of obscuration measured in NGC 5506.

To broadly characterize the prominence of the soft X-ray emission with respect to the total X-ray spectrum, we have adopted the soft X-ray luminosity (0.1-2 keV) and the hard X-ray luminosity (2-10 keV) ratio as in Bianchi et al. (2009a), based on the fact that luminosities are only slightly affected by the choice of the model. Bianchi et al. (2009a) found that NLSy1 have luminosity ratios higher than unity and are distributed at higher values with respect to BLSy1, showing a soft X-ray emission dominance in NLSy1. This is not confirmed in our sample, where only in IGR J19378-0617 and NGC 4748 (see Table 6) the luminosity ratio is only slightly higher than 1, suggesting that the hard X-ray selection of the sample may reduce the bias introduced by the ROSAT soft X-ray selection of NLSy1.

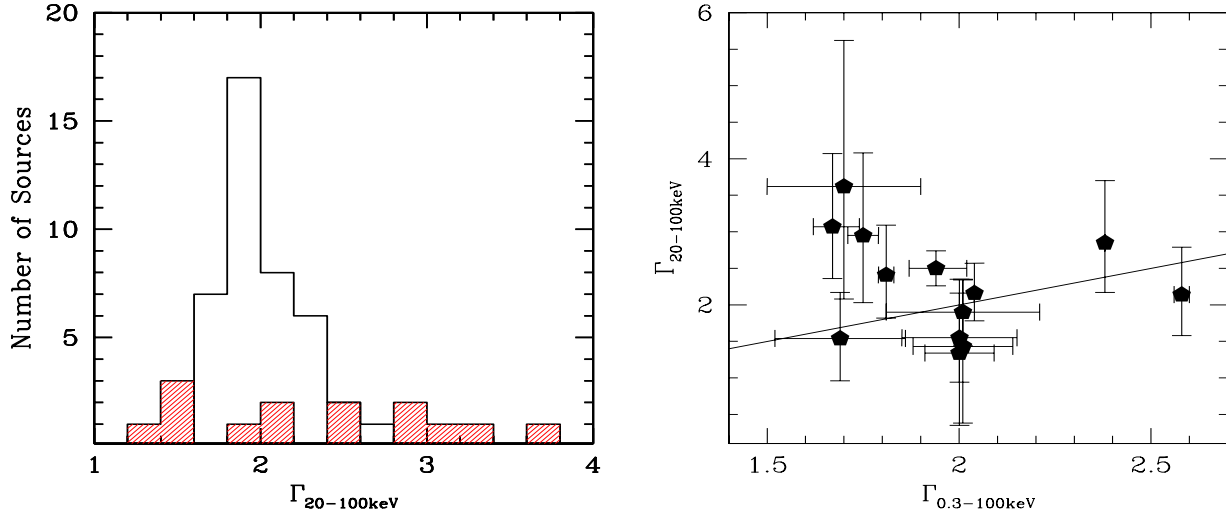


Figure 4. Left panel: Distribution of the 20-100 keV photon index for our sample of NLSy1 (shaded histogram) and a sample of hard X-ray selected BLSy1 (Molina et al. in preparation). Right panel: 20-100 keV photon index versus the 0.3-100 keV broad-band photon index in NLSy1.

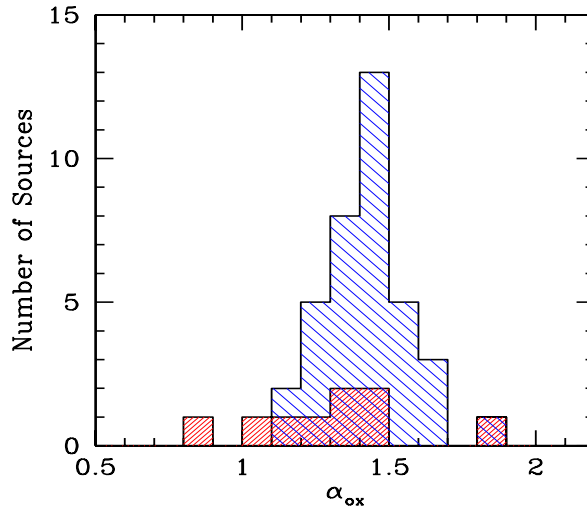


Figure 5. Distribution of the optical-to-X-ray spectral slope α_{ox} in our sample (right-hand shaded histogram) and in Grupe et al. (2010) NLSy1 sample (left-hand shaded histogram).

4.4 Hard X-ray variability

In Bird et al. (2010), sources variability has been searched for at revolution level, at revolution sequence (sequence of consecutive similar pointings) and then also by optimizing the source detection time scale; this is the so-called "bursticity" analysis. In fact, light curve for each source has been scanned with variable time window to obtain the best source significance in the 18-60 keV band, then both duration and time-interval of the best detection period have been recorded. The ratio of the maximum significance on any time-scale to the significance for the whole data set define the "bursticity" so that a value of 1 is associated to persistent sources for which all data set can be used to increase its significance while a values greater than 1 indicates variability and

hence part of the data can be neglected to enhance the significance. Of course the higher is the bursticity values, the strongest is the source variability. Only one source in our list, IGR J16426+6536, has increased its flux by a factor of ~ 3 on less than one day time scale, the rest of the sample does not show burst-like events. It must be noted that the source significance is often at the sensitivity limit not allowing a proper characterization of the long term variability properties within their *INTEGRAL* light curves. NGC 4051 is the only source in our sample which belongs to the list of variable *INTEGRAL* sources edited by Telezhinsky et al. (2010).

A comparison between the fourth IBIS catalogue and BAT 54 months shows that fluxes in the 20-100 keV energy

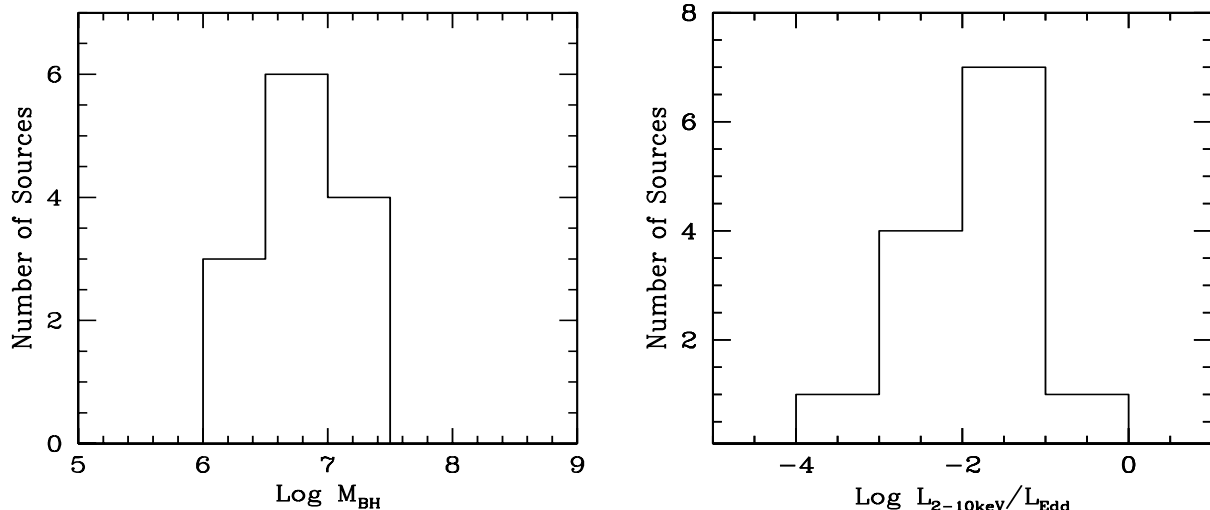


Figure 6. Left panel: Log black hole mass distribution in NLSy1. Right panel: Log $L_{2-10\text{keV}}/L_{\text{Edd}}$ ratio distribution.

range are almost consistent, with a maximum difference by a factor of 3, as in the case of 1H 0323+342. The large variability in 1H 0323+342 has already been discussed (Foschini et al. 2009) and expected given the blazar-like nature of this source. We should bear in mind that the IBIS fluxes are averaged in the period between 2002 and 2008, while BAT fluxes from 2004 till 2009, therefore data partially overlaps. However, we notice that BAT fluxes tend to be systematically lower with respect to IBIS fluxes (except for NGC 5506). In a systematic comparison between IBIS and BAT data performed on a complete sample of *INTEGRAL* sources, it has been found that indeed there is a tendency for BAT fluxes to be lower with respect to the IBIS fluxes, especially for dimmer sources (as NLSy1 are): this can be interpreted as a sign of some systematics between the two instruments (Molina et al. in preparation).

On shorter time-scales, i.e., within a single *Suzaku*/PIN observation taken in 2005, NGC 4051 shows only moderate variability in the 15-40 keV light curve, from 2.4 to 2.9×10^{-11} ergs $\text{cm}^{-2} \text{s}^{-1}$ in the low and high flux states, respectively (Terashima et al. 2009); this values are consistent with the average *INTEGRAL* flux. The hard X-ray flux has increased during a second *Suzaku* observation in 2008, where a strong excess over a power law at energies above 20 keV is found, some fraction of which also appears to vary with the power-law continuum (Miller et al. 2010). Mrk 766 was observed twice above 10 keV by the PDS on board *BeppoSAX* with a flux of 3×10^{-11} erg $\text{cm}^{-2} \text{s}^{-1}$ showing evidence of flux variability (Landi et al. 2005). The 12-40 keV *Suzaku* light curve of Mrk 766 (Turner et al. 2007) is consistent with a constant flux at around 0.01 counts s^{-1} , which translates into a 12-40 keV flux of 4×10^{-12} erg $\text{cm}^{-2} \text{s}^{-1}$, 40% lower than the *INTEGRAL* and BAT average flux in that energy range. The 20-100 keV *Suzaku* flux of IGR J16185-5928 is 1.5×10^{-11} erg $\text{cm}^{-2} \text{s}^{-1}$ (Miniutti et al. in preparation), consistent with the average *INTEGRAL* value. Also for Swift J2127.4+5654, the IBIS average flux is perfectly consistent with the *Suzaku* PIN flux ($F_{20-100\text{keV}} = 4.2 \times 10^{-11}$ erg $\text{cm}^{-2} \text{s}^{-1}$). NGC 5506 is known to be one of

the most variable AGN in the X-ray domain on short-time scales (e.g., ~ 300 s, Dewangan & Griffiths, 2005), while on long-time scale a systematic variation on its spectral slope is found (Guainazzi et al. 2010). At energies above 20 keV, a monitoring campaign with HEXIT (Manchanda 2006) reveals a variation by a factor of 10 in flux and also spectral variability. The 15-136 keV *BeppoSAX* flux of 17×10^{-11} ergs $\text{cm}^{-2} \text{s}^{-1}$ (Deluit 2004) is in agreement with the average *INTEGRAL* value. Summarizing, in those sources with multiple targeted observations, variability is often found (three out of five sources in our sample), suggesting that variability is a common trait in NLSy1 not only in X-rays but also in the hard X-rays domain.

5 DISCUSSION

5.1 Fraction of hard X-ray NLSy1

In the fourth IBIS catalogue, 723 hard X-ray Galactic and extra-Galactic sources are listed, nearly 30% of these sources had an "unknown" classification/identification at the time of the publication of the catalogue. The continuous follow-up campaigns for the identification of the new hard X-ray sources is now reducing this fraction. As by August 2010 (Masetti et al. 2010), nearly 35% of the sources in the catalogue have been identified as AGN (258), with 207 objects classified as Seyfert galaxies (98 as type 1 and 109 as type 2). Therefore, in the *INTEGRAL* hard X-ray sky, NLSy1 constitute $\sim 14\%$ of the type 1 Seyfert population and $\sim 5\%$ of the AGN population. However, it should be considered that the hard X-ray sky is not uniformly covered by the *INTEGRAL* exposures: 70% of the sky around the Galactic plane region is covered to better than 1 mCrab sensitivity, compared to the 5 mCrab level of 90% of the extragalactic regions (Bird et al. 2010). This is likely introducing a bias against the number of AGN detections, which is indeed increasing during the latest years when the survey is covering more extragalactic fields. The AGN (and NLSy1) number is therefore to be intended as a lower limit. On the other

hand, extragalactic sources in the *Swift*/BAT sky largely outnumber the galactic sources, because of the uniform sky coverage (e.g., Cusumano et al. 2010, Tueller et al. 2010). In the Palermo *Swift*/BAT catalogue (54 months), 735 AGN are listed, of which 472 are Seyfert galaxies. The lack of a fine Seyfert classification does not allow a proper determination of the NLSy1 fraction. To our knowledge, 14 among the 307 type 1 Seyfert galaxies reported are indeed NLSy1, reducing their fraction to $\geq 5\%$ among type 1 AGN and only to $\geq 2\%$ among the total AGN population. This low fraction could be possibly ascribed to the BAT lower exposure observation on each target or sky area. Moreover, the better IBIS sensitivity limit compared to the BAT instrument allows the detection of faint hard X-ray AGN such as NLSy1. If we consider the complete hard X-ray sample in the 20-40 keV band by Malizia et al. (2009), the fraction of NLSy1 is $\sim 11\%$ among type 1 Seyfert galaxies and $\sim 6\%$ among all AGN in the sample. This is probably the more realistic estimate of the NLSy1 fraction in the hard X-ray sky.

An unbiased estimate of the fraction of NLSy1 among AGN is difficult to obtain, since this number strongly depends on the sample selection and the energy range used. During the ROSAT soft X-ray survey a large number of NLSy1 have been discovered; Grupe (2004) estimated a fraction of $\sim 46\%$ of NLSy1 while Hasinger et al. (2000) only $\sim 1\%$. An optically selected sample provides a NLSy1 fraction of $\sim 15\%$ among the type 1 AGN population (Zhou et al. 2006, Williams et al. 2002), in agreement with the hard X-ray fraction (5-15%) which suggests that hard X-rays are efficient in selecting NLSy1.

5.2 Black Hole mass, Eddington ratio and radio-loudness

The peculiar properties of NLSy1 have been commonly associated to their small black hole masses and relative high Eddington ratios. Black hole masses are usually estimated through mass-radius relations (see Table 1), the latter derived from the optical continuum luminosity (Kaspi et al. 2000). However it must be kept in mind that large uncertainties affect these estimates. The distribution of the black hole masses in our sample (Figure 6, left panel) peaks at $\sim 10^7 M_\odot$, confirming the findings that NLSy1 host preferentially small black holes and possibly suggesting that the hard X-ray origin of the sample is not introducing any particular selection effect in the black hole mass range. This result is similar to that found in an X-ray selected sample where Bianchi et al. (2009b) have shown that NLSy1 have the smallest BH masses when compared to BLSy1. The 2-10 keV luminosity and Eddington luminosity ratios (Figure 6, right panel) also point to highly accreting systems, although hard X-ray NLSy1 seem to occupy the lower Eddington ratios tail of the NLSy1 population distribution (see Bianchi et al. 2009b). A correlation between the photon index and the Eddington ratio has been found by several authors (Grupe et al. 2010, Risaliti et al. 2009, Shemmer et al. 2008). Hard X-ray NLSy1 may occupy the "flat- Γ /low Eddington ratio" part of this correlation with respect to the soft X-ray selected NLSy1 which may be found in the "steep- Γ /high Eddington ratio" part.

Grupe et al. (2010) have also shown that for a sample of X-ray selected NLSy1 and BLSy1 the distribution of

the reddening corrected optical-to-X-ray spectral slopes α_{ox} was very similar. To check for a possible difference introduced by the hard X-ray selection, we have compared the α_{ox} distribution of the X-ray selected NLSy1 from Grupe et al. (2010) (left-hand shaded histogram in Figure 5) with that of the *INTEGRAL* NLSy1 (right-hand shaded histogram). A Kolmogorov-Smirnov (K-S) test results in a probability $P = 0.057$ of a random result, indicating that the distributions are not significantly different. We find two extreme cases of a very X-ray-to-optical loud source IRAS 15091-2107 ($\alpha_{ox} = 0.9$) and an X-ray quiet source Swift J2127.4+5654. However, the strong Galactic extinction for both galaxies may not guarantee a correct estimate of the dereddened flux; indeed, as shown by Grupe et al. (2010), the reddening correction influences the final measurements and distributions.

A small black hole mass of $10^7 M_\odot$ is residing in 1H 0323+342 which is a gamma-ray source, detected by *Fermi*, with a spectral energy distribution typical of BL Lac objects. This is at odds with the evidence that radio-loud AGN are generally associated with the most massive black holes and are known to reside mostly in elliptical galaxies (e.g. McLure & Jarvis 2004, Dunlop et al. 2003). Interestingly, at least three sources in our sample are ellipticals (IRAS 15091-2107, IGR J16385-2057 and IGR J19378-0617) characterized by black hole masses $< 10^7 M_\odot$ and, they are radio sources. In Table 1 we report the radio fluxes at 1.4 or 5 GHz. The strongest radio sources in our sample are 1H 0323+342 and NGC 5506. However, if we calculate the X-ray radio-loudness parameter $R_X \equiv L_\nu(R)/L(2-10 \text{ keV})$, only 1H 0323+342 can strictly be considered as radio-loud ($\log R_X = -2.7$) if we assume the more conservative radio-quiet versus radio-loud boundary as defined in Panessa et al. (2007). Otherwise, if we assume the limit set by Terashima & Wilson (2003) to $\log R_X = -4.5$, source in the sample should be considered as radio-loud, except for IGR J16385-2057, IGR J19378-0617 and Swift J2127.4+5654. The radio-loudness parameters obtained from the low angular resolution integrated flux should, however, be taken with caution, since it has been shown that observations at high angular resolution can resolve $> 40\%$ of the larger scale emission, resulting in a much reduced core radio luminosity and a lower radio-loudness parameter, as shown from interferometric measurements of NGC 4051 which provide $\log R_X = -5.8$, suggesting that the central AGN is very radio-quiet (Giroletti & Panessa 2009). Considering the 11 NLSy1 with radio measurements, the fraction of radio-loud sources in our sample is likely $\sim 9\%$, consistently with Komossa (2007) who found that 7% of the NLSy1 galaxies in their sample were radio-loud and only 2.5% "very" radio loud ($R > 100$). This result also confirms the search for NLSy1 in the FIRST survey (the Faint Images of the Radio Sky at 20 cm survey; Becker et al. 1995), where a decline of the NLSy1 fraction is observed toward high R-values, i.e., the NLSy1 fraction falls down to 10% in moderately strong radio AGNs (Zhou et al. 2006).

6 CONCLUSIONS

Hard X-ray NLSy1 look very heterogeneous in their broadband properties, displaying a broad range of hard X-ray (20-100 keV) photon indices, flatly distributed from quite flat (~ 1.3) to very steep (~ 3.6) slopes. At these energies

no clear separation between the BLSy1 and NLSy1 slopes distributions is found, although the hard X-ray selection may introduce a bias against faint steep spectrum sources. Steeper photon indices for NLSy1 are instead found when considering the broad-band spectra. In only one source, Swift J2127.4+5654, a high energy cut-off is measured at a relatively low value ($E_{cut-off} \sim 50$ keV), and the reflection fraction constrained to $R=1.0^{+0.5}_{-0.4}$, confirming previous measurements (Malizia et al. 2008, Miniutti et al. 2009). Apparently, the hard X-ray selection is not efficient in detecting strong soft X-ray NLSy1 as, indeed, only one source, IGR J19378-0617, shows a dominant and strongly variable soft X-ray component. The presence of fully or partially covering absorption is quite frequently measured in the spectra (in four out of ten sources analyzed in this work). When the spectral quality is good (i.e., with XMM-Newton data), we almost always detect the presence of an Fe line (showing from narrow to moderately broad profiles). A proper determination of the reflection strength is limited by the non simultaneity of the X-ray and hard X-ray observations. This is particularly true in this class of sources where X-ray variability (in flux and spectrum) is strong, both at short and long timescales, as here demonstrated by the XMM-Newton light curves and in those sources where multiple observations were available. *INTEGRAL* and BAT hard X-rays average fluxes are consistent, with a maximum flux variation of $\sim 30\%$. Overall, the average X-ray spectrum of NLSy1 looks more similar to the BLSy1 spectrum when the sources are selected at hard X-ray rather than soft X-rays (e.g., *ROSAT*).

We estimate that the fraction of NLSy1 in the hard X-ray sky is about 10-15% of the type 1 AGN population, in agreement with the optically selected sample fraction. The black hole mass distribution of NLSy1 selected in hard X-rays peaks at $10^7 M_{\odot}$ and the Eddington ratios distribution peaks at 10^{-2} , suggesting that hard X-ray NLSy1 occupy the lower tail of Eddington ratios distribution of NLSy1. When data are available, NLSy1 in our sample are radio emitting objects, though not radio-loud, except for 1H 0323+342 which is a blazar-like NLSy1.

ACKNOWLEDGMENTS

We thank the referee, Dirk Grupe, for his useful comments and suggestions which helped us improving our paper. We thank Alessandro Maselli for his precious contribution to the *Swift*/UVOT data analysis. FP and RL acknowledge support by *INTEGRAL* ASI I/033/10/0 and ASI/INAF I/009/10/0. GM thanks the Spanish Ministry of Science and Innovation for support through grants AYA2009-08059 and AYA2010-21490-C02-02.

REFERENCES

- Abdo, A. A., et al. 2009, *ApJ*, 707, L142
 Ajello, M., et al. 2008, *ApJ*, 673, 96
 Arnaud, K. A. 1996, *Astronomical Data Analysis Software and Systems V*, 101, 17
 Barthelmy, S. D., et al. 2005, *Space Sci. Rev.*, 120, 143
 Bassani, L., et al. 2006, *ApJ*, 636, L65
 Becker, R. H., White, R. L., & Helfand, D. J. 1995, *ApJ*, 450, 559
 Becker, R. H., White, R. L., & Edwards, A. L. 1991, *ApJS*, 75, 1
 Bennett, C. L., et al. 2003, *ApJS*, 148, 1
 Bianchi, S., Guainazzi, M., Matt, G., Fonseca Bonilla, N., & Ponti, G. 2009a, *A&A*, 495, 421
 Bianchi, S., Bonilla, N. F., Guainazzi, M., Matt, G., & Ponti, G. 2009b, *A&A*, 501, 915
 Bird, A. J., et al. 2010, *ApJS*, 186, 1
 Bird, A. J., et al. 2007, *ApJS*, 170, 175
 Boller, T., Tanaka, Y., Fabian, A., Brandt, W. N., Gallo, L., Anabuki, N., Haba, Y., & Vaughan, S. 2003, *MNRAS*, 343, L89
 Boller, T., et al. 2002, *MNRAS*, 329, L1
 Boller, T., Brandt, W. N., & Fink, H. 1996, *A&A*, 305, 53
 Brandt, W. N., Mathur, S., & Elvis, M. 1997, *MNRAS*, 285, L25
 Burrows, D. N., et al. 2005, *Space Sci. Rev.*, 120, 165
 Butler, S. C., et al. 2009, *ApJ*, 698, 502
 Comastri, A. 2000, *NewAR*, 44, 403
 Condon, J. J., Cotton, W. D., Greisen, E. W., Yin, Q. F., Perley, R. A., Taylor, G. B., & Broderick, J. J. 1998, *AJ*, 115, 1693
 Cusumano, G., et al. 2010, *A&A*, 510, A48
 Deluit, S. J. 2004, *A&A*, 415, 39
 Denney, K. D., et al. 2009, *ApJ*, 702, 1353
 de Rosa, A., Bassani, L., Ubertini, P., Panessa, F., Malizia, A., Dean, A. J., & Walter, R. 2008, *A&A*, 483, 749
 Dewangan, G. C., & Griffiths, R. E. 2005, *ApJ*, 625, L31
 Dietrich, M., Crenshaw, D. M., & Kraemer, S. B. 2005, *ApJ*, 623, 700
 Dunlop, J. S., McLure, R. J., Kukula, M. J., Baum, S. A., O'Dea, C. P., & Hughes, D. H. 2003, *MNRAS*, 340, 1095
 Fabian, A. C., Miniutti, G., Gallo, L., Boller, T., Tanaka, Y., Vaughan, S., & Ross, R. R. 2004, *MNRAS*, 353, 1071
 Foschini, L., Maraschi, L., Tavecchio, F., Ghisellini, G., Gliozzi, M., & Sambruna, R. M. 2009, *Advances in Space Research*, 43, 889
 Gallimore, J. F., Axon, D. J., O'Dea, C. P., Baum, S. A., & Pedlar, A. 2006, *AJ*, 132, 546
 Gallo, L. C. 2006, *MNRAS*, 368, 479
 Gehrels, N., et al. 2004, *ApJ*, 611, 1005
 George, I. M., Turner, T. J., Yaqoob, T., Netzer, H., Laor, A., Mushotzky, R. F., Nandra, K., & Takahashi, T. 2000, *ApJ*, 531, 52
 Gierliński, M., & Done, C. 2004, *MNRAS*, 349, L7
 Giroletti, M., & Panessa, F. 2009, *ApJ*, 706, L260
 Goldwurm, A., et al. 2003, *A&A*, 411, L223
 Goodrich, R. W. 1989, *ApJ*, 342, 224
 Grupe, D., Komossa, S., Leighly, K. M., & Page, K. L. 2010, *ApJS*, 187, 64
 Grupe, D., & Mathur, S. 2004, *ApJ*, 606, L41
 Grupe, D. 2004, *AJ*, 127, 1799
 Guainazzi, M., Bianchi, S., Matt, G., Dadina, M., Kaastra, J., Malzac, J., & Risaliti, G. 2010, *MNRAS*, 406, 2013
 Halpern, J. P. 2006, *ATel*, 847
 Hasinger, G., Lehmann, I., Schmidt, M., Gunn, J. E., Schneider, D. P., Giacconi, R., Trümper, J., & Zamorani, G. 2000, *NewAR*, 44, 497
 Hill, J. E., et al. 2004, *Proc. SPIE*, 5165, 217

- Kaspi, S., Smith, P. S., Netzer, H., Maoz, D., Jannuzi, B. T., & Givon, U. 2000, *ApJ*, 533, 631
- Komossa, S. 2007, *The Central Engine of Active Galactic Nuclei*, 373, 719
- Komossa, S., & Xu, D. 2007, *ApJ*, 667, L33
- Landi, R., Bassani, L., Malizia, A., Stephen, J. B., Bazzano, A., Fiocchi, M., & Bird, A. J. 2010, *MNRAS*, 403, 945
- Landi, R., Malizia, A., & Bassani, L. 2005, *A&A*, 441, 69
- Leighly, K. M. 1999, *ApJS*, 125, 317
- Longinotti, A. L., Cappi, M., Nandra, K., Dadina, M., & Pellegrini, S. 2003, *A&A*, 410, 471
- Malizia, A., Bassani, L., Sguera, V., Stephen, J. B., Bazzano, A., Fiocchi, M., & Bird, A. J. 2010, *MNRAS*, 408, 975
- Malizia, A., Stephen, J. B., Bassani, L., Bird, A. J., Panessa, F., & Ubertini, P. 2009, *MNRAS*, 399, 944
- Malizia, A., et al. 2008, *MNRAS*, 389, 1360
- Manchanda, R. K. 2006, *Advances in Space Research*, 38, 1387
- Marconi, A., Axon, D. J., Maiolino, R., Nagao, T., Pastorini, G., Pietrini, P., Robinson, A., & Torricelli, G. 2008, *ApJ*, 678, 693
- Masetti, N., et al. 2010, *A&A*, 519, A96
- Masetti, N., et al. 2009, *A&A*, 495, 121
- Masetti, N., et al. 2008, *A&A*, 482, 113
- Masetti, N., et al. 2007, *A&A*, 470, 331
- Masetti, N., Morelli, L., Palazzi, E., et al. 2006, *A&A*, 459, 21
- Mason, K. O., et al. 2001, *A&A*, 365, L36
- Mathur, S., Kuraszewicz, J., & Czerny, B. 2001, *NewA*, 6, 321
- McLure, R. J., & Jarvis, M. J. 2004, *MNRAS*, 353, L45
- Miller, L., Turner, T. J., Reeves, J. N., Lobban, A., Kraemer, S. B., & Crenshaw, D. M. 2010, *MNRAS*, 403, 196
- Miniutti, G., Panessa, F., de Rosa, A., Fabian, A. C., Malizia, A., Molina, M., Miller, J. M., & Vaughan, S. 2009, *MNRAS*, 398, 255
- Molina, M., et al. 2009, *MNRAS*, 399, 1293
- Moretti, A., et al. 2004, *Proc. SPIE*, 5165, 232
- Nagar, N. M., Oliva, E., Marconi, A., & Maiolino, R. 2002, *A&A*, 391, L21
- Nandra, K., George, I. M., Mushotzky, R. F., Turner, T. J., & Yaqoob, T. 1997, *ApJ*, 477, 602
- Nikolajuk, M., Czerny, B., & Gurynowicz, P. 2009, *MNRAS*, 394, 2141
- Osterbrock, D. E., & De Robertis, M. M. 1985, *PASP*, 97, 1129
- Osterbrock, D. E., & Pogge, R. W. 1985, *ApJ*, 297, 166
- Panessa, F., et al. 2008, *A&A*, 483, 151
- Panessa, F., Barcons, X., Bassani, L., Cappi, M., Carrera, F. J., Ho, L. C., & Pellegrini, S. 2007, *A&A*, 467, 519
- Ponti, G., et al. 2010, *MNRAS*, 406, 2591
- Ponti, G., Miniutti, G., Cappi, M., Maraschi, L., Fabian, A. C., & Iwasawa, K. 2006, *MNRAS*, 368, 903
- Reynolds, C. S. 1997, *MNRAS*, 286, 513
- Risaliti, G., Young, M., & Elvis, M. 2009, *ApJ*, 700, L6
- Rodriguez-Ardila, A., Pastoriza, M. G., Donzelli, C. J. 2000, *ApJS*, 126, 63
- Roming, P. W. A., et al. 2005, *Space Sci. Rev.*, 120, 95
- Shemmer, O., Brandt, W. N., Netzer, H., Maiolino, R., & Kaspi, S. 2008, *ApJ*, 682, 81
- Sulentic, J. W., Zwitter, T., Marziani, P., & Dultzin-Hacyan, D. 2000, *ApJ*, 536, L5
- Tanaka, Y., Boller, T., Gallo, L., Keil, R., & Ueda, Y. 2004, *PASJ*, 56, L9
- Teleshinsky, I., Eckert, D., Savchenko, V., Neronov, A., Produit, N., & Courvoisier, T. J.-L. 2010, *A&A*, 522, A68
- Terashima, Y., et al. 2009, *PASJ*, 61, 299
- Terashima, Y. & Wilson, A. S. 2003, *ApJ*, 583, 145
- Tueller, J., et al. 2010, *ApJS*, 186, 378
- Tueller, J., Markwardt, C. B., Skinner, G. K., Baumgardner, W. H., & Swift BAT Survey Team 2009, *Bulletin of the American Astronomical Society*, 41, 269
- Turner, T. J., Miller, L., Reeves, J. N., & Kraemer, S. B. 2007, *A&A*, 475, 121
- Turner, T. J., George, I. M., & Netzer, H. 1999, *ApJ*, 526, 52
- Ubertini, P., et al. 2003, *A&A*, 411, L131
- Ulvestad, J. S., Antonucci, R. R. J., & Goodrich, R. W. 1995, *AJ*, 109, 81
- Uttley, P., Taylor, R. D., McHardy, I. M., Page, M. J., Mason, K. O., Lamer, G., & Fruscione, A. 2004, *MNRAS*, 347, 1345
- Véron-Cetty, M.-P., & Véron, P. 2006, *A&A*, 455, 773
- Wandel, A., Peterson, B. M., & Malkan, M. A. 1999, *ApJ*, 526, 579
- Wang, T., & Lu, Y. 2001, *A&A*, 377, 52
- Whalen, D. J., Laurent-Muehleisen, S. A., Moran, E. C., & Becker, R. H. 2006, *AJ*, 131, 1948
- Williams, R. J., Pogge, R. W., & Mathur, S. 2002, *AJ*, 124, 3042
- Winkler, C., et al. 2003, *A&A*, 411, L1
- Winter, L. M., Mushotzky, R. F., Tueller, J., & Markwardt, C. 2008, *ApJ*, 674, 686
- Yuan, W., Zhou, H. Y., Komossa, S., Dong, X. B., Wang, T. G., Lu, H. L., & Bai, J. M. 2008, *ApJ*, 685, 801
- Zhou, H., et al. 2007, *ApJ*, 658, L13
- Zhou, H., Wang, T., Yuan, W., Lu, H., Dong, X., Wang, J., & Lu, Y. 2006, *ApJS*, 166, 128
- Zhou, H.-Y., & Wang, T.-G. 2002, *ChJAA*, 2, 501